

 Open access • Posted Content • DOI:10.1101/2020.02.05.935833

## Large-scale RNAi screening uncovers new therapeutic targets in the human parasite *Schistosoma mansoni* — [Source link](#)

[Jipeng Wang](#), [Carlos Paz](#), [Gilda Padalino](#), [Avril Coghlan](#) ...+6 more authors

**Institutions:** [University of Texas Southwestern Medical Center](#), [Aberystwyth University](#), [Wellcome Trust Sanger Institute](#)

**Published on:** 06 Feb 2020 - [bioRxiv](#) (Cold Spring Harbor Laboratory)

**Topics:** [Schistosoma mansoni](#) and [Transplantation](#)

Related papers:

- [The Tao survivorship of schistosomes: implications for schistosomiasis control.](#)
- [Current and prospective chemotherapy options for schistosomiasis](#)
- [Changes in microRNA expression in response to \*Schistosoma japonicum\* infection.](#)
- [Advances in the Study of Schistosomiasis: The Postgenomic Era](#)
- [Protein tyrosine kinases as new potential targets against human schistosomiasis.](#)

Share this paper:    

View more about this paper here: <https://typeset.io/papers/large-scale-rnai-screening-uncovers-new-therapeutic-targets-32ra5arozf>

1 **Large-scale RNAi screening uncovers new therapeutic targets in the human parasite**  
2 ***Schistosoma mansoni***

3

4 Jipeng Wang<sup>1\*</sup>, Carlos Paz<sup>1\*</sup>, Gilda Padalino<sup>2</sup>, Avril Coghlan<sup>3</sup>, Zhigang Lu<sup>3</sup>, Irina Gradinaru<sup>1</sup>,  
5 Julie N.R. Collins<sup>1</sup>, Matthew Berriman<sup>3</sup>, Karl F. Hoffmann<sup>2</sup>, James J. Collins III<sup>1†</sup>.

6

7

8 <sup>1</sup>Department of Pharmacology, UT Southwestern Medical Center, Dallas, Texas 75390

9 <sup>2</sup>Institute of Biological, Environmental and Rural Sciences (IBERS), Aberystwyth University,  
10 Aberystwyth, Wales, UK.

11 <sup>3</sup>Wellcome Sanger Institute, Wellcome Genome Campus, Hinxton, Cambridge CB10 1SA, UK

12 \*Equal Contribution

13

14

15

16

17

18

19

20

21

22

23 †To whom correspondence should be addressed

24 [JamesJ.Collins@UTSouthwestern.edu](mailto:JamesJ.Collins@UTSouthwestern.edu)

25 UT Southwestern Medical Center

26 Department of Pharmacology

27 6001 Forest Park. Rd.

28 Dallas, TX 75390

29 United States of America

30 **ABSTRACT**

31 **Schistosomes kill 250,000 people every year and are responsible for serious morbidity in 240**  
32 **million of the world's poorest people. Despite their profound global impact, only a single**  
33 **drug (praziquantel) is available to treat schistosomiasis, highlighting the need to better**  
34 **understand schistosome biology to drive the development of a new generation of**  
35 **therapeutics. A major barrier to this goal is the paucity of large-scale datasets exploring**  
36 **schistosome gene function. Here, we describe the first large-scale RNA interference screen**  
37 **in adult *Schistosoma mansoni* examining the function of over 2000 genes representing**  
38 **approximately 20 percent of the protein coding genome. More than 250 genes were found to**  
39 **have phenotypes affecting neuromuscular function, tissue integrity, stem cell maintenance,**  
40 **and parasite survival. Leveraging these data, we bioinformatically prioritized several**  
41 **compounds with *in vitro* activity against parasites and validated p97, a component of the**  
42 **ubiquitin proteasome system, as a drug target in the worm. We further reveal a potentially**  
43 **druggable protein kinase-signaling module involving the TAO and STK25 kinases that are**  
44 **essential for maintaining the transcription of muscle-specific mRNAs. Importantly, loss of**  
45 **either of these kinases results in paralysis and death of schistosomes following surgical**  
46 **transplantation into a mammalian host. We anticipate this work will invigorate studies into**  
47 **the biology of these poorly studied organisms and expedite the development of new**  
48 **therapeutics to treat an important neglected tropical disease.**

49

50 Genome sequences are available for the major species of medically-relevant schistosomes<sup>1-</sup>  
51 <sup>3</sup>; nevertheless, studies of gene function have been limited to relatively small numbers of genes<sup>4,5</sup>.  
52 To address this issue, we developed a platform for large-scale RNAi screening on adult  
53 schistosomes (**Fig. 1a**). To establish the efficacy of this platform to detect phenotypes in adult *S.*  
54 *mansoni*, we prioritized a list of 2,320 of the worm's ~10,000 protein coding genes, including  
55 those encoding enzymes, cell-surface receptors, ion channels, and hypothetical proteins of  
56 unknown function (**Supplementary Table 1**). After filtering for genes expressed in adult  
57 schistosome somatic tissues using existing expression datasets<sup>6</sup>, we performed Polymerase Chain  
58 Reactions (PCR) from schistosome cDNA, generated dsRNAs, and performed RNAi by treating  
59 adult pairs of male and female worms with five dsRNA treatments over the course of a 30-day  
60 experiment (**Fig. 1b**). After filtering genes that either did not amplify during PCR steps, or failed  
61 to generate sufficient concentrations of dsRNA, a total of 2,216 genes were screened  
62 (**Supplementary Table 1**).

63 These parasites live in the veins surrounding the host intestines, and attachment to the  
64 vascular endothelium is essential *in vivo* for parasites to be kept from being swept away in the  
65 blood and trapped in host organs. Since detachment from an *in vitro* tissue culture substrate has  
66 been shown to precede more deleterious phenotypes<sup>7</sup>, and since under our *in vitro* culture  
67 conditions, healthy parasites firmly attached to the substrate using a combination of their oral and  
68 ventral suckers (**Supplementary Video 1**), we reasoned that substrate attachment would be a  
69 useful quantitative metric to define RNAi treatments that affect parasite vitality and predict *in vivo*  
70 survival. Therefore, during our 30-day experiments we monitored parasites every 48 hours for  
71 substrate attachment and any other visible defects. Schistosomes possess adult somatic stem cells,  
72 called neoblasts, that rejuvenate key parasite tissues, including the intestine and tegument (skin)<sup>6,8</sup>,

73 and are likely to be essential for long-term parasite survival in the blood. The parasites also contain  
74 large numbers of proliferative germline stem cells (GSCs) in their reproductive organs<sup>8</sup> which are  
75 essential for producing eggs that represent the central driver of parasite-induced pathology *in vivo*<sup>9</sup>.  
76 Therefore, we also monitored the maintenance of neoblasts and GSCs by labeling with the  
77 thymidine analog EdU prior to the conclusion of the experiment (**Fig. 1b**). Due to the variable rate  
78 at which the reproductive organs of female worms degenerate during *in vitro* culture<sup>10</sup>, stem cell  
79 proliferation was only monitored in male worms. At the conclusion of this initial screen we  
80 performed two major quality control steps for RNAi treatments resulting in attachment- or stem  
81 cell- related phenotypes. First, we confirmed the identity of every gene producing a phenotype by  
82 DNA sequencing. Second, where possible, we examined the specificity of our RNAi knockdown  
83 by designing new oligonucleotides targeting a non-overlapping region of genes that produced  
84 phenotypes (**Fig. 1a, Extended Data Fig. 1**). To be considered a “hit” a gene must have shown a  
85 fully penetrant phenotype in three independent experiments. These studies identified 195 genes  
86 that were essential for parasite attachment, and thus potentially essential for worm survival *in vivo*.  
87 In addition to facilitating parasite substrate attachment, we also observed that 121 of these 195  
88 genes were associated with other visible phenotypes including tissue and intestinal edema (36),  
89 head (26) and/or tegument (78) degeneration, muscular hypercontraction (6), and complete  
90 cessation of movement (death) (36) (**Fig. 2a, Supplementary Table 2**). In addition to these genes,  
91 we found that RNAi of an additional 66 genes resulted in stem cell maintenance defects but caused  
92 no other visible phenotypes (*e.g.*, substrate attachment) suggesting a selective role in stem cell  
93 maintenance (**Supplementary Table 3, Extended Data Fig. 2**).

94         Of the 66 genes essential for stem cell survival over 90% (60/66) led to defects in the  
95 maintenance of both neoblasts and proliferative cells in the male testes (**Extended Data Fig. 2**).

96 However, in a minority of cases some genes appeared to play more significant roles in maintaining  
97 proliferative cells in either the male germ line (e.g., a RAD51 homolog) or the neoblasts (e.g.,  
98 *fgfrA*, a previously-described FGF receptor homolog<sup>8</sup>) (**Fig. 2b**). In addition to genes necessary  
99 for cell cycle progression (e.g., *polo-like kinase*), Gene Ontology enrichment analysis highlighted  
100 genes important for protein translation, including gene products involved in ribosomal structure,  
101 tRNA aminoacylation, and rRNA processing as important regulators of proliferative cell  
102 maintenance (**Fig. 2c, Extended Data Fig. 3**). Although this could reflect an enhanced sensitivity  
103 of actively proliferating cells to alterations in protein translation, recent work has highlighted “non-  
104 housekeeping” roles for translational regulators in controlling stem cell function<sup>11</sup>. Thus, it is worth  
105 exploring whether specific roles for translational control exist for regulating schistosome stem cell  
106 function.

107         Similar to previous whole organism large-scale RNAi studies in other metazoa<sup>12,13</sup>, we  
108 found that a large fraction of the 195 genes essential for parasite vitality (attachment) share  
109 sequence similarity (BLAST *E*-value < 1e-5) with genes in other organisms including *C. elegans*  
110 (91%), *Drosophila* (93%), the planarian *Schmidtea mediterranea* (97%), and humans (93%)  
111 (**Supplementary Table 4**). Some of these 195 schistosome genes with detachment phenotypes  
112 have *C. elegans*/*D. melanogaster* orthologs that lack any phenotypes (**Supplementary Table 5**);  
113 such genes could regulate novel schistosome-specific biology or represent opportunities for studies  
114 of *S. mansoni* to shed light on the function of poorly characterized animal gene families. Further  
115 examination of genes with attachment phenotypes by Gene Ontology analyses revealed that  
116 although this dataset was enriched for genes encoding regulators of protein transport and mRNA  
117 transcription (**Fig. 2c, Extended Data Fig. 3**), the dominant group of enriched genes were those  
118 encoding components necessary for protein turnover via the ubiquitin-proteasome system (UPS)

119 **(Fig. 2c, Extended Data Fig. 3)**. RNAi and pharmacological studies have implicated proteolysis  
120 by the proteasome as important for larval, and, more recently adult viability *in vitro*<sup>14,15</sup>. However,  
121 our data points to a much broader requirement for UPS components in these worms. Indeed,  
122 inspection of our RNAi dataset found that key components from virtually every arm of the UPS  
123 were required for adult parasite vitality during *in vitro* culture including: E1/E2 ubiquitin ligases  
124 and Deubiquitinating Enzymes (DUBs), the AAA-ATPase p97 that delivers proteins to the  
125 proteasome<sup>16</sup>, and nearly all regulatory and catalytic subunits of the proteasome complex<sup>17</sup> **(Fig.**  
126 **2d)**. Indeed, RNAi of nearly all of UPS components resulted in extensive tissue degeneration and  
127 in some cases (e.g., *p97(RNAi)*) adult parasite death **(Extended Data Fig. 4)**. Taken together, these  
128 data suggest that disruption not just of proteasome function, but any critical UPS components,  
129 results in reduced schistosome vitality *in vitro*.

130 To determine if any genes associated with attachment phenotypes encoded proteins  
131 targeted by existing pharmacological agents, we performed a combination of manual searches of  
132 the literature and bioinformatic comparisons with the ChEMBL database<sup>18</sup> **(Supplementary**  
133 **Table 6)**. This analysis uncovered 205 compounds potentially targeting 49 *S. mansoni* proteins.  
134 To gauge the utility of this approach to prioritize compounds with activity on adult parasites, we  
135 selected 14 of these compounds **(Supplementary Table 7)**, including: FDA-approved drugs (e.g.,  
136 Ixazomib, Panobinostat), drugs currently or previously explored in clinical trials (e.g., CB-5083,  
137 HSP990), or experimental compounds with activity in rodent models of disease (e.g.,  
138 Thapsigargin, NMS-873). We then examined their activities on worms cultured *in vitro* using an  
139 automated worm movement tracking platform<sup>19</sup> and by measuring the effects on parasite  
140 attachment following drug treatment. This analysis found that more than half of the compounds  
141 tested (8/14) on worms at 10  $\mu$ M reduced parasite movement >75% and half of the compounds

142 (7/14) caused fully penetrant substrate attachment defects by D7 post-treatment (**Fig. 3a-b,**  
143 **Supplementary Video 2**). Among the compounds that emerged from these studies was  
144 simvastatin, an HMG-CoA reductase inhibitor, that was previously shown to have effects on  
145 parasites both *in vitro* and *in vivo*<sup>20</sup>. We also evaluated these compounds on post-infective larvae  
146 (schistosomula), observing that 7 had profound effects on parasite movement (**Supplementary**  
147 **Table 8**), suggesting the potential of these compounds to target multiple schistosome life-cycle  
148 stages. Consistent with our observation that UPS function is critical for schistosome vitality (**Fig.**  
149 **2d-f**), we found that the proteasome inhibitor ixazomib caused profound effects on both  
150 schistosome movement (**Fig. 3a**) and attachment (**Fig. 3b**), mirroring a recent report using the  
151 proteasome inhibitor bortezomib<sup>14</sup>. However, among compounds with the most potent effects on  
152 adult parasites were inhibitors of the UPS component p97: CB-5083, an ATP-competitive  
153 inhibitor<sup>21</sup>, and NMS-873, an allosteric inhibitor<sup>22</sup>, that both had sub-micromolar effects on adult  
154 worm movement ( $EC_{50} = 0.93 \mu\text{M}$  for NMS-873 and  $0.16 \mu\text{M}$  for CB-5083) (**Extended Data Fig.**  
155 **5**). Similar to the death observed following long-term *p97* RNAi treatment (**Fig 2a**), both NMS-  
156 873 and CB-5083 led to death *in vitro* (**Supplementary Video 3**). Despite their differing  
157 mechanisms of p97 inhibition (ATP-competitive vs allosteric), we noted similar deformations in  
158 the structure of the parasite tegument following treatment with either CB-5083 and NMS-873,  
159 suggesting that these compounds have similar pharmacological effects on the parasite (**Fig. 3c**).  
160 Given the prominent role for the UPS in schistosomes (**Fig. 2c-d**), we assessed if NMS-873 and  
161 CB-5083 affected UPS function by measuring the accumulation of ubiquitinated proteins using an  
162 antibody that recognizes K48 polyubiquitinated proteins marked for proteasome-mediated  
163 destruction<sup>23</sup>. Not only did we observe the accumulation of polyubiquitinated proteins following  
164 RNAi of *p97*, treatment of schistosomes with either CB-5083 or NMS-873 enhanced anti-K48

165 polyubiquitin labeling (**Fig. 3d**). We observed similar accumulation of polyubiquitinated proteins  
166 following either RNAi of *proteasome subunit beta type-2* or treatment with ixazomib (**Extended**  
167 **Data Fig. 5**). These effects on the degradation of ubiquitinated proteins appeared to be specific to  
168 inhibition of UPS function, rather than a non-specific effect due to reduced worm vitality, as  
169 treatment with the sarco/endoplasmic reticulum Ca<sup>2+</sup>-ATPase inhibitor thapsigargin, which also  
170 caused profound effects on worms (**Fig 3a, 3b**), did not alter the accumulation of polyubiquitinated  
171 proteins (**Extended Data Fig. 5**).

172 To determine if UPS function is broadly required for adult schistosomes *in vivo*, we  
173 depleted UPS components using RNAi and surgically transplanted these worms into the  
174 mesenteric veins of recipient mice (**Extended Data Fig. 6**) to measure parasite egg deposition in  
175 host tissues and parasite survival<sup>7</sup>. Following hepatic portal perfusion, we recovered about 55%  
176 of control RNAi-treated worms originally transplanted (**Fig. 2e, Extended Data Fig. 6**) and these  
177 parasites established patent infections depositing large number of eggs into the livers of recipient  
178 mice (**Fig. 2f, Extended Data Fig. 6**). In contrast, we failed to recover parasites following hepatic  
179 portal perfusion from mice receiving *p97* (**Fig. 2e**) or *proteasome subunit beta type-2* (**Extended**  
180 **Data Fig. 6**) RNAi-treated worms. Additionally, the livers in these mice were devoid of eggs, as  
181 a consequence, we observed no signs of egg-induced granulomas (**Fig. 2f, Extended Data Fig. 6**).  
182 We did, however, observe RNAi-treated parasites at various stages of being infiltrated by host  
183 immune cells in the livers of recipient mice (**Fig. 2g, Extended Data Fig. 6**), suggesting these  
184 parasites are unable to remain in the portal vasculature and are cleared via the immune system in  
185 the liver. Thus, several components of the UPS are essential for schistosome survival *in vivo*.  
186 Recent studies from a variety of human parasites have highlighted the potential for therapeutically  
187 targeting UPS function by inhibition of the proteasome<sup>14,24,25</sup>. Our data suggest that targeting

188 another critical (and druggable<sup>21,22</sup>) mediator of UPS function (*i.e.*, p97) may have therapeutic  
189 potential, not just against schistosomes, but against a variety of important human parasites.

190 Another prominent group of potentially druggable targets to emerge from our RNAi screen  
191 were protein kinases, 19 of which led to defects in either parasite attachment or stem cell  
192 maintenance. The most striking protein kinase-related phenotypes resulted from RNAi of two  
193 STE20 serine-threonine kinases: *tao* and *stk25*, which are homologs of the human TAO1/2/3 and  
194 STK25/YSK1 protein kinases, respectively. RNAi of either of these kinases led to rapid  
195 detachment from the substrate (**Extended Data Fig. 7**) and a concomitant posterior paralysis and  
196 hypercontraction of the body, such that the parasites were shorter than controls and took on a  
197 distinctive banana-shaped morphology (**Fig 4a-b, Supplementary Video 4**). Aside from RNAi  
198 of *stk25* and *tao*, this banana-shaped phenotype was unique, only observed in our screening  
199 following RNAi of a CCM3/PDCD10 homolog (Smp\_031950), a known heterodimerization  
200 partner with the mammalian STK25 kinase<sup>26</sup>. We failed to observe death of either *stk25*- or *tao*-  
201 depleted parasites during *in vitro* culture; however, following surgical transplantation we noted a  
202 significant reduction in the recovery of *tao* or *stk25* RNAi-treated parasites from recipient mice  
203 and these recipient mice displayed little signs of egg-induced granuloma formation (**Extended**  
204 **Data Fig. 7**). Thus, both *tao* and *stk25* appear to be essential for schistosome survival *in vivo*.

205 Given the unique and specific nature of the *stk25* and *tao* associated “banana” phenotype  
206 we reasoned that these kinases may be acting in concert to mediate similar signaling processes in  
207 the worm. Recent data suggests that the *Drosophila* STK25 ortholog (GCK3) is a substrate of  
208 TAO and that these proteins function in a signaling cascade essential for tracheal development<sup>27</sup>.  
209 Consistent with these studies, we too observed that recombinant *S. mansoni* STK25 (SmSTK25)  
210 could serve as a substrate for the *S. mansoni* TAO (SmTAO) in an *in vitro* kinase assay (**Extended**

211 **Data 8)**. The human STK25 is activated by phosphorylation of a conserved threonine residue  
212 within its activation loop<sup>28</sup>. By mass spectrometry we observed that this conserved threonine  
213 within the predicted SmSTK25 activation loop (T<sup>173</sup>) was phosphorylated following incubation of  
214 recombinant SmTAO with catalytically inactive SmSTK25 in the presence of ATP (**Extended**  
215 **Data 8)**. To explore this observation in more detail we performed western blotting on *in vitro*  
216 kinase reactions using an antibody that recognizes phosphorylation of the conserved threonine in  
217 the activation loop of vertebrate and invertebrate STK25 orthologs<sup>27</sup>. Validating the specificity of  
218 this antibody of against phosphorylated T<sup>173</sup> on SmSTK25, we detected robust SmSTK25 T<sup>173</sup>  
219 autophosphorylation following an *in vitro* kinase reaction; this signal was abrogated when ATP  
220 was omitted from the reaction or when the SmSTK25 catalytic K<sup>48</sup> residue was mutated to R (**Fig.**  
221 **4c, Extended Data 10)**. Consistent with our mass spectrometry results, we detected robust  
222 phosphorylation of T<sup>173</sup> when recombinant SmTAO was incubated with kinase dead SmSTK25  
223 (**Fig. 4c**), suggesting that SmTAO can phosphorylate a residue key for the activation of the  
224 mammalian STK25.

225         Given their phenotypic similarities and our biochemical observations, we reasoned that the  
226 schistosome TAO and STK25 might be acting in a signaling module to mediate critical processes  
227 in the parasite. To define these processes, we performed transcriptional profiling on RNAi-treated  
228 parasites just prior to the timepoint in which we observed detachment and hypercontraction (Day  
229 6 and Day 9 for *tao* and *stk25* RNAi treatments, respectively) (**Extended Data Fig. 9)**. We  
230 reasoned that transcriptional changes common to both *stk25* and *tao* RNAi data sets would provide  
231 details about any processes regulated by these proteins. Consistent with the model that these  
232 kinases cooperate in the parasite, we found that expression of differentially regulated genes  
233 following RNAi of either *tao* or *stk25* were highly correlated (**Fig. 4d**) and that more than half of

234 these differentially regulated genes were common in both datasets (**Extended Data Fig. 9,**  
235 **Supplementary Table 9**). Importantly, RNAi of either *tao* or *stk25* was specific, not affecting  
236 expression of the other kinase gene of this pair (**Fig. 4c, d**). To better understand the genesis of  
237 the phenotype associated with loss of *tao* or *stk25*, we examined the tissue-specific expression of  
238 differentially-regulated genes on an adult schistosome single cell expression atlas using cells from  
239 schistosome somatic tissues<sup>29</sup>. Strikingly, we found that roughly 40% (51/129) of the most down-  
240 regulated genes following *tao* and *stk25* RNAi (Log<sub>2</sub> Fold Change < -0.5, adjusted *p*-value <  
241 0.00001) were specific markers of parasite muscle cells (**Extended Data Fig. 10, Supplementary**  
242 **Table 9**). Indeed, nearly half of all mRNAs specifically-enriched in muscle cells (60/135) from  
243 this single cell atlas, including key muscle contractile proteins (*e.g.* Troponin subunits Actins,  
244 Myosin light/heavy chains, and Tropomyosin), were significantly down-regulated following RNAi  
245 of both *tao* and *stk25* (**Fig. 4e, Extended Data Fig. 10, Supplementary Table 10**). Importantly,  
246 these transcriptional effects appeared to be largely specific to parasite muscles, since  
247 comparatively few markers specific to other major somatic organ systems (neurons, gut,  
248 parenchyma) were affected by RNAi of these kinases (**Fig. 4e, Extended Data Fig. 10,**  
249 **Supplementary Table 10**). In principle, loss of muscle-specific mRNAs could be due to either  
250 loss of muscle cells or down-regulation of muscle-specific mRNAs. To distinguish between these  
251 possibilities, we performed labeling with phalloidin to mark F-actin in schistosome muscle fibers  
252 and *in situ* hybridization to detect muscle-specific mRNAs. Within a few days of RNAi-treated  
253 parasites adopting their banana-shaped phenotype, we noted a dramatic reduction in the expression  
254 of mRNAs encoding the contractile proteins Tropomyosin 1 and a Myosin Light Chain by *in situ*  
255 hybridization (**Fig. 4f**), but observed no major qualitative defects in phalloidin labeling in the  
256 muscle fibers within anterior or posterior body wall muscles (**Fig 4g, Extended Data Fig. 8**).

257 Thus, it appears that these kinases are required to maintain the transcription of a large number of  
258 muscle-specific mRNAs in intact muscle cells. Interestingly, we noted that the heads of *tao* and  
259 *stk25* RNAi parasites, which retained their capacity for movement (**Supplementary Video 4**),  
260 partially maintained the expression of muscle-specific mRNAs (**Fig. 4f**). Thus, there appears to  
261 be a relationship between the maintenance of muscle-specific mRNA expression and locomotion.  
262 Taken in their entirety, our data are consistent with the model that STK25 and TAO kinases  
263 cooperate (perhaps with TAO directly activating STK25) in the schistosome to mediate a signaling  
264 cascade essential for sustaining transcription of muscle-specific mRNAs. As a consequence, loss  
265 of either SmSTK25 or SmTAO activity results in muscular function defects and this compromises  
266 parasite survival *in vivo*. Although the essentiality of the three mammalian TAO homologs is  
267 unclear, whole body knockouts of mouse STK25 are homozygous viable displaying no obvious  
268 deleterious phenotypes<sup>30</sup>. Thus, SmSTK25 function appears to be a schistosome-specific liability  
269 for survival when compared to mammals. Given this, and the druggable nature of kinases, we  
270 suggest that SmSTK25 represents a high-value target for therapeutic intervention.

271 Technological advances have paved the way for large-scale analyses of gene function in  
272 protozoan parasites<sup>31-33</sup>, but, unfortunately, comparable resources have not yet materialized for any  
273 helminth parasite. Here, we have performed the largest systematic analysis to date of gene function  
274 in schistosomes, examining roughly 20 percent of the protein coding genes in the parasite. Our  
275 RNAi studies, together with bioinformatics, have allowed us to effectively prioritize targets  
276 essential *in vivo* (e.g., STK25, TAO, and p97) and potential specific inhibitors with *in vitro*  
277 activities on worms (**Fig 3a-b**). Thus, future efforts should not only explore compounds our  
278 bioinformatic approaches have already uncovered (**Supplementary Table 6**), but also larger  
279 libraries of compounds with known molecular targets (e.g., the REFRAME collection<sup>34</sup>). Such

280 studies are likely to be an efficient means to identify existing drugs for potential repurposing  
281 against schistosomes. Not only does this study enhance our understanding of schistosome biology,  
282 and serve as a template for conducting further genome-scale studies of schistosome gene function,  
283 it provides a new lens to prioritize genes of interest in other medically- and agriculturally-  
284 important parasitic flatworms (e.g., tapeworms and flukes). Collectively, we anticipate this study  
285 will expedite the discovery of new anthelmintics.

286

287 **Fig1. Platform for large-scale RNAi screening in *S. mansoni*.**

288 a. Pipeline for large-scale RNAi screening in *S. mansoni*.

289 b. Double-stranded RNA treatment regime over the course of the 30-day treatment period of adult  
290 worms. During the entire experiment parasites are monitored for visible abnormalities and at D29  
291 EdU is added to media to label proliferative cells in the parasites.

292

293 **Fig2. Summary of RNAi phenotypes.**

294 a. Categories of RNAi phenotypes observed. *kin-17* (Smp\_023250), *cog* (Smp\_132980), *p97*  
295 (Smp\_018240), *c44* (Smp\_136260), *prpf4b* (Smp\_068960), *gtf2f1* (Smp\_088460), *stk25*  
296 (Smp\_096640).

297 b. EdU-labeling (yellow) showing proliferative cells in somatic tissues and the testes. RNAi of  
298 DNA polymerase epsilon subunit (Smp\_124120) leads to loss of all proliferative cells, whereas  
299 *rad51* (Smp\_124230) or *fgfrA* (Smp\_175590) lead to a selective reduction in the testes and soma,  
300 respectively.

301 c. Gene Ontology analysis examining the biological processes of genes required for either stem  
302 cell maintenance or substrate attachment.

303 d. A large fraction of genes resulting in visible phenotypes were associated with components of  
304 the Ubiquitin Proteasome System (UPS). Left, cartoon of the UPS. Colored UPS components  
305 correspond to genes associated with visible phenotypes.

306 Scale bars: a, 100  $\mu$ m; b, 200  $\mu$ m

307

308 **Fig3. Compounds prioritized from RNAi studies have effects on schistosomes *in vitro*.**

309 a. Compounds (red text) predicted to target schistosome proteins (blue text) essential for parasite  
310 vitality from RNAi studies were examined at 10  $\mu$ M for their effects on worm motility. Parasites  
311 were incubated with compounds and movement assessed after 72 hrs. Praziquantel (PZQ, 10  $\mu$ M  
312 in 0.1% DMSO) and DMSO (0.1%) were used as positive control and negative controls,  
313 respectively. Dashed line shows threshold for 75% reduction in worm motility. Error bars  
314 represent standard deviation of the mean motility scores.  $n = 12$  (three biological replicates, each  
315 compound was tested in duplicate - each replicate containing a pair of adult worms/well).

316 b. Heatmap showing time course measuring the fraction of male worms attached to the substrate  
317 over a 7-day period following treatment of worms with compounds for 72 hours as in a.

318 c. Treatment with either CB-5083 or NMS-873 at 10  $\mu$ M (72 hrs) caused severe blebbing and  
319 delamination of the tegument.

320 d. Western Blot for K-linked polyubiquitinated proteins. RNAi of *p97* or treatment of worms with  
321 *p97* inhibitors caused an increase in the accumulation of polyubiquitinated proteins.  
322 Representative from 3 experiments.

323 e. Percent recovery of male parasites treated with dsRNA specific to *p97* (Smp\_018240;  $n = 8$   
324 transplants) or an irrelevant dsRNA (*control*;  $n = 8$  transplants) following surgical transplantation  
325 of parasites into mice. \*\*\*\*\*,  $p < 0.0001$ , t-test

326 f. Hematoxylin and Eosin staining of livers from recipient mice that received either control or  
327 *p97(RNAi)*. Schistosome egg-induced granulomas in livers were observed in control RNAi  
328 recipient mice, but not in *p97(RNAi)* recipient mice. Counts of eggs per liver section are shown in  
329 top left,  $n=3$ .

330 g. Transplanted parasites from *p97(RNAi)* treatments were found trapped and in various stages of  
331 degeneration in livers of recipient mice.

332 Scale bar: c, f, g, 100  $\mu$ m.

333  
334 **Fig4. The protein kinases SmSTK25 and SmTAO are essential to maintain muscular**  
335 **function**

- 336 a. RNAi of *stk25* or *tao* causes parasites to become hypercontracted.  
337 b. *stk25* and *tao* RNAi-treated parasites are shorter than control RNAi-treated worms. >19  
338 parasites monitored over 4 experiments.  $p < 0.0001$ , t-test.  
339 c. Western blot to detect phosphor-T173 (p-SmSTK25) or total SmSTK25 following an *in vitro*  
340 kinase reaction with recombinant proteins in the presence or absence of ATP. Active SmSTK25  
341 can autophosphorylate T173, as can SmTAO when incubated with kinase dead SmSTK25  
342 (kdSmSTK25). T173 phosphorylation was dependent on ATP. kdSmTAO represents kinase dead  
343 SmTAO. Representative of 2 experiments.  
344 d. Dot plot showing the relationship between the differentially expressed genes following either  
345 *stk25* or *tao* RNAi-treatment. These expression profiles were highly correlated ( $R = 0.9$ ,  $p <$   
346  $0.0001$ ).  
347 e. Heatmap showing that many muscle-specific transcripts were down-regulated following RNAi  
348 of *tao* or *stk25*.  
349 f. *in situ* hybridization to detect the expression of *tropomyosin 1* (Smp\_340760) and a myosin light  
350 chain (Smp\_132670) following RNAi of *tao* or *stk25* at D13.  
351 g. Phalloidin labeling to mark F-actin in muscle cells of RNAi treated parasites at D13 indicating  
352 that muscle fibers are intact at this timepoint after depletion of *tao* or *stk25*.  
353 Scale bars: a, 500  $\mu\text{m}$ ; f, 100  $\mu\text{m}$ ; g, 20  $\mu\text{m}$ .  
354

355 **Supplementary Information Guide.**

- 356 **Supplementary Table 1.** Information of 2,320 genes selected for RNAi screening.  
357 **Supplementary Table 2.** Details of 195 genes with detachment phenotypes.  
358 **Supplementary Table 3.** Details of 66 genes with phenotypes in EdU incorporation.  
359 **Supplementary Table 4.** Similarity of schistosome genes with phenotypes with gene products  
360 from other organisms by BLAST.  
361 **Supplementary Table 5.** *S. mansoni* genes with detachment phenotypes, whose *C. elegans* and  
362 *D. melanogaster* orthologs lack phenotypes in WormBase/FlyBase  
363 **Supplementary Table 6.** Human homologs of *S. mansoni* RNAi hits and their potential inhibitors.  
364 **Supplementary Table 7.** Details of 14 selected inhibitors to test on schistosome.  
365 **Supplementary Table 8.** Evaluation of compound activity on schistosomula  
366 **Supplementary Table 9.** Analysis of transcriptional changes following *stk25* or *tao* RNAi  
367 treatment by DESeq. Second tab shows which somatic cell clusters the most down-regulated  
368 ( $p < 0.00001$  Log<sub>2</sub> Fold Change  $< -0.5$ ) genes following *stk25* or *tao* RNAi treatment are expressed.  
369 **Supplementary Table 10.** Analysis of expression of somatic tissue-specific markers following  
370 *stk25* or *tao* RNAi treatment. Tissue-specific markers down-regulated (Log<sub>2</sub> Fold Change  $< 0$  and  
371  $p_{\text{Adj}} < 0.000001$ ) following both *stk25* and *tao* RNAi-treatments are highlighted in red.  
372

373 **Supplementary Video 1. Adult worms after 30 days of *in vitro* treatment with control**  
374 **dsRNA.** On day 30, worms were physically active and firmly attached to the bottom of the dish.

375 **Supplementary Video 2. Parasites died in 72 hours *in vitro* after inhibition by CB-5083 or**  
376 **NMS-873.** Adult worms were dead following 72 hours of treatment with 1  $\mu$ M CB-5083 or 5  
377  $\mu$ M NMS-873. Tegmental damage was observed on these worms. DMSO was used as a control.

378 **Supplementary Video 3. *stk25/tao* RNAi treated worms become hypercontracted and**  
379 **paralyzed by D13 following dsRNA treatment.**

380 **Supplementary Video 4. Effects of various compounds on parasites.** Parasites were treated  
381 with compounds for 72 hours at a concentration of 10  $\mu$ M. We observed various worm defects  
382 ranging from death, to tissue degeneration, and detachment from the substrate. DMSO and PZQ  
383 were used as negative and positive controls, respectively.

384

385

386

387

## 388 **Acknowledgements**

389 We thank Megan McConathy, Caroline Furrh, and Dr Giampaolo Pagliuca for technical assistance and  
390 Fiona Hunter and Nicolas Bosc for advice about retrieving data from ChEMBL. Mice and *B. glabrata* snails  
391 were provided by the National Institute of Allergy and Infectious Diseases (NIAID) Schistosomiasis  
392 Resource Center of the Biomedical Research Institute (Rockville, MD, USA) through National Institutes  
393 of Health (NIH)-NIAID Contract HHSN2722010000051 for distribution through BEI Resources. The work  
394 was supported by the National Institutes of Health R01AI121037 (JJC), the Welch Foundation I-1948-  
395 20180324 (JJC), the Burroughs Wellcome Fund (JJC), and the Wellcome Trust 107475/Z/15/Z  
396 (JJC/KFH/MB).

397

## 398 **Methods**

399

### 400 **Parasites**

401 Adult *S. mansoni* (NMRI strain) (6–7 weeks post-infection) or juvenile worms (4–5 weeks post-infection) were  
402 harvested from infected mice by hepatic portal vein perfusion with 37°C DMEM (Mediatech, Manassas, VA) plus 8%  
403 Horse Serum and heparin. Parasites were rinsed in DMEM + plus 8% Horse Serum and cultured (37°C/5% CO<sub>2</sub>) in  
404 Basch's Medium 169<sup>35</sup> and 1× Antibiotic-Antimycotic (Gibco/Life Technologies, Carlsbad, CA 92008). Experiments  
405 with and care of vertebrate animals were performed in accordance with protocols approved by the Institutional Animal  
406 Care and Use Committee (IACUC) of UT Southwestern Medical Center (approval APN: 2017-102092).

407

### 408 **Initial RNAi screening**

409 Primers were designed to amplify ~700 bp fragment using BatchPrimer3  
410 <http://batchprimer3.bioinformatics.ucdavis.edu/index.html>. For genes shorter than 700 bp, primers were designed to  
411 cover as much of the transcript as possible. For reverse transcription of double stranded RNAs, a T7 promoter  
412 sequence (GAATTTAATACGACTCACTATA) was added to the 5' end of each oligo. To facilitate DNA sequencing  
413 of cDNAs associated with RNAi phenotypes, we added a *NotI* or *AscI* restriction enzyme site between the T7 and  
414 gene-specific sequences on the forward and reverse oligos, respectively. These oligos were synthesized and packaged  
415 in 96-well plates and used for PCR using adult schistosome cDNA as a template. 5 µL of PCR products were then  
416 used for *in vitro* transcription to generate dsRNA in 100 µL as previously described<sup>36</sup>. After overnight incubation at  
417 37 °C, dsRNAs were annealed by a successive 3-min gradient incubation at 95 °C, 75 °C, and 55 °C, then cooled down  
418 at room temperature for 5 min. The presence and size of PCR products and dsRNA were all analyzed by agarose gel  
419 electrophoresis and samples stored at -20 °C. For RNAi treatments, approximately 5 pairs of adult parasites were  
420 placed in 3 mL Basch 169 media in a 12-well plate and treated with 20 µL dsRNA at D0, D2, D9, D16 and D23. To  
421 examine cell proliferation, the media were supplemented with EdU (10 µM) at D29. On day 30, videos were captured  
422 for RNAi treatments that caused visible RNAi phenotypes and after video acquisition all parasites were fixed and  
423 processed for EdU detection<sup>8</sup>. During the entire 30D RNAi treatment regime, media was changed every 1-2 days and  
424 worm attachment and morphological changes were monitored. Videos RNAi treatments causing visible phenotypes  
425 can be found at: [https://datadryad.org/stash/share/R4pxckHwhrBqUyfmkuH2FhhRJzdp\\_wKlBkZpVCP8QE](https://datadryad.org/stash/share/R4pxckHwhrBqUyfmkuH2FhhRJzdp_wKlBkZpVCP8QE).

426

427 To validate hits from the initial RNAi screening, the original PCR products were digested with *NotI* (NEB) for 30 min  
428 at 37 °C, gel purified (Zymoclean Gel DNA Recovery Kit), and sequenced with a T7 primer. Sequences of genes  
429 validated by sequencing were uploaded into BatchPrimer3 to design new primers that amplify a fragment sharing no  
430 overlap with the PCR products from the initial RNAi screening. In cases where genes' sequences were too short to  
431 design new oligos, we retained the original primer sequences. These primers were synthesized without further  
432 modification, used to generate PCR products, and then inserted into pJC53.2 using TA cloning<sup>36</sup>. These plasmids  
433 were purified from *E. coli*, validated by sequencing, and used as a template to generate dsRNA. We then repeated the  
434 RNAi treatment regime used in the original screen.

435

### 436 **Parasite labelling and imaging**

437 Whole-mount in situ hybridization<sup>6</sup>, EdU detection<sup>8</sup>, and phalloidin staining<sup>37</sup> were performed as previously described.  
438 For in situ hybridization, riboprobes were generated from cDNA fragments amplified using primers for tropomyosin-  
439 1 (Smp\_340760, gagaagagaatgctatggaaagagc/cctcattttgtagtttagacttgacg) or myosin light chain (Smp\_132670,  
440 gttgctctgttaagtaaacatggg/gttagtctctaatgtcttgattgcc). Brightfield images of in situ hybridizations and worm  
441 morphology/movement were imaged using a Zeiss AxioZoom V16 (Zeiss, Germany) equipped with a transmitted

442 light base and a Zeiss AxioCam 105 Color camera. Fluorescent images were acquired using a Nikon A1+ laser  
443 scanning confocal microscope.

444

#### 445 **Transplantation of dsRNA-treated Schistosomes**

446 Parasites 4–5 weeks post-infection were recovered from mice and treated with 30 µg/ml dsRNA for 4 days in Basch  
447 Media 169 with a daily replacement of media and dsRNA and surgically transplanted into naïve mice as previously  
448 described<sup>7</sup>. On day 26 post-transplantation, mice were sacrificed and perfused to recover parasites. Male and female  
449 parasites were counted and livers were removed and fixed for 30–40 hours in 4% formaldehyde in PBS. The  
450 percentage of parasite recovery was determined by dividing the number of male worms transplanted by the number  
451 of male parasites recovered following perfusion. Livers from individual mice were sectioned and processed for  
452 Hematoxylin and Eosin staining by the UT Southwestern Molecular Pathology Core.

453

#### 454 **Detection of polyubiquitinated proteins by western blot**

455 For RNA interference, 10 single-sex male adult worms (6 weeks post infection) were treated with 30 µg/mL dsRNA  
456 in Basch Media 169 for 8 days. Media and dsRNA were changed daily. On day 9, worms were collected and flash  
457 frozen. For drug treatment, 10 male adult worms (single or paired with females) were supplemented with either  
458 DMSO, NMS 873 or CB 5083. After 24hrs, male parasites were separated from females using 0.25% tricaine in Basch  
459 Media 169 and flash frozen. Male worm samples were homogenized with a pestle in 50 µL lysis buffer containing  
460 2 x sample buffer, protease inhibitor cocktail (Roche, cOmplete Mini, EDTA-free Tablets) and 10mM DTT. The  
461 lysates were then sonicated on high for 5 min (30 sec on, 30 sec off) using a Bioruptor UCD-200. Lysates were  
462 centrifuged for 5 min at 10,000 g to remove debris. Total protein was measured using the Detergent Compatible  
463 Bradford Assay (Pierce). 35 µg of protein samples denatured in SDS Sample buffer (95°C for 5min) were separated  
464 on a Bio-Rad 4-20% TGX Stain-Free gel along with Precision Plus Protein Dual Color Standards (Bio-Rad) as a  
465 marker. Proteins were then transferred to a nitrocellulose membrane (Bio-Rad) and confirmed by Ponceau S  
466 staining. The membrane was blocked in a 1:5 solution of Li-Cor Odyssey Blocking buffer in PBS for 1hr before being  
467 immunoblotted overnight at 4°C with 1:500 K48-linkage Specific Polyubiquitin Antibody (Cell Signaling  
468 Technology, 4289S) and 0.01 µg/mL mouse anti-actin antibody (Developmental Studies Hybridoma Bank, JLA20)  
469 diluted in a 1:5 solution of Li-Cor Odyssey Blocking buffer in PBS. The membrane was washed 3x in TBST and then  
470 incubated in 1:5 Li-Cor Odyssey Blocking buffer containing the secondary antibodies (1:10,000 Li-Cor, 925-68071,  
471 goat anti-rabbit IRDye 680 RD, and 1:20,000 Li-Cor, 925-32280, goat anti-mouse IgM IRDye 800CW) for 1hr at RT.  
472 The blot was washed in TBST 3x before being imaged on a Li-Cor Odyssey Infrared Imager.

473

#### 474 **Compound prioritization**

475 To manually search for existing drugs targeting “detachment” hits from our RNAi screen, we performed protein-  
476 protein BLAST against the *Homo sapiens* proteome to find the closest human homolog to our RNAi hits. We then  
477 manually searched a variety of databases (*e.g.*, genecards, google, DrugBank, Therapeutic Targets Database) and  
478 chemical vendors (*e.g.*, seleckchem) for inhibitors against these human proteins. In each instance, we consulted the  
479 published literature to give preference to compounds likely to be selective for a given target. If several such drugs  
480 were available, preference was given to those that were also orally bioavailable and/or FDA approved/in clinical trials.  
481 For larger-scale discovery of compounds, the *S. mansoni* protein sequences of genes with ‘detachment’ phenotypes  
482 were used to search the ChEMBL database<sup>18</sup>, to identify compounds predicted to interact with them. To do this, we  
483 followed the protocol previously described<sup>38</sup> with the following differences. First, for each *S. mansoni* gene, we  
484 identified its top BLASTP hit among all ChEMBL targets, as well as any ChEMBL targets having BLAST hits with  
485 *E*-values within 10<sup>5</sup> of the top hit’s *E*-value; and then extracted from ChEMBL the drugs/compounds with bioactivities  
486 against those particular ChEMBL targets. Second, when calculating the ‘toxicology target interaction’ component of  
487 a compound’s score, we checked whether ChEMBL predicted with probability >0.5 that the compound interacts with  
488 one of 108 toxicology targets curated from<sup>39-41</sup>.

489

#### 490 **Evaluation of effects of compounds on worms**

491 *in vitro* evaluation of selected compounds (single-point concentrations, 10 µM in 0.1% DMSO) on adult movement  
492 was replicated three times using a single worm pair per well (two technical replicates each time, n = 12), as previously  
493 described<sup>42</sup>. Worm pairs co-cultivated with DMSO (0.1% negative control) and Praziquantel (PZQ) (10 µM in 0.1%  
494 DMSO; positive control) were included in each experiment. Following incubation at 37°C for 72 hrs in a humidified  
495 atmosphere containing 5% CO<sub>2</sub>, a digital image processing-based system was used for the assessment of parasite  
496 motility. Both hardware and software components of this system (WormassayGP2) were inspired by the digital  
497 macroscopic imaging apparatus previously described<sup>19</sup>, with minor modifications to the source code (supporting USB

498 video class, UVC, camcorders and the High Sierra MacOS) and user interface (allowing manual manipulations to  
499 recording duration). A dose-response titration (10  $\mu\text{M}$  – 0.156  $\mu\text{M}$ ) of CB-5083 and NMS-873 was performed to  
500 assess adult worm anti-schistosomal potencies. Each titration point was performed in triplicate (a pair of worms for  
501 each replicate). Worm movement was recorded with WormassayGP2, as mentioned above. Mean motility scores were  
502 calculated for each titration point and dose-response curves were derived in comparison to worms co-cultured in  
503 DMSO (0.1% v/v; negative control; 100% motility) and PZQ (10  $\mu\text{M}$  in 0.1% DMSO; positive control; 0% motility).  
504 Anti-schistosomula activities of the selected compounds were assessed using the high-content imaging platform  
505 Roboworm as previously described<sup>42,43</sup>. Compounds (reconstituted in dimethyl sulfoxide, DMSO; 10 mM stock  
506 concentration) were initially tested at two different concentration points (10  $\mu\text{M}$  and 50  $\mu\text{M}$ , in 0.625% DMSO) along  
507 with negative (0.625% DMSO) and positive controls (PZQ at 10  $\mu\text{M}$  final concentration in 0.625 % DMSO).  
508 Schistosomula/compound co-cultures were then incubated at 37°C for 72 h in a humidified atmosphere containing 5%  
509 CO<sub>2</sub> before phenotype and motility metrics were assessed. Two-fold titrations (10  $\mu\text{M}$ , 5  $\mu\text{M}$ , 2.5  $\mu\text{M}$ , 1.25  $\mu\text{M}$  and  
510 0.625  $\mu\text{M}$ ) were subsequently conducted for all compounds consistently identified as hits at 10  $\mu\text{M}$  in the primary  
511 screens. Single point schistosomula screens (10  $\mu\text{M}$ ) were repeated three times whereas dose response titrations were  
512 performed twice (in each screen two technical replicates were included). Phenotype and motility scores deriving from  
513 the titration of each compound were collected to generate approximate EC<sub>50</sub>s using GraphPad Prism. To quantify  
514 adult worm attachment to the substrate following drug treatment, freshly perfused adult worms were sorted into a 6-  
515 well plate with 3 mL Basch 169 media and cultured overnight. The following day (D0) unattached worms removed  
516 and compounds were added to the media to a final concentration of 10  $\mu\text{M}$ . Media and drug were replaced on D1 and  
517 D2. Media with no drug was added on D3 and D5. Parasite attachment was monitored from D0 to D7.

#### 518 519 **RNaseq for *stk25* and *tao* RNAi-treated worms**

520 To examine gene expression changes following loss of *tao* or *stk25*, 10 adult worm pairs were placed into 6-well plates  
521 and cultured in 3 mL Basch 169 supplemented with 30  $\mu\text{g}/\text{mL}$  dsRNA for 3 days. Media and dsRNA were replaced  
522 daily. On D3, dsRNA-containing media was removed and worms were maintained in 6 mL Basch 169 media that was  
523 replaced every other day. On day 6 (*tao*(RNAi)) or D9 (*stk25*(RNAi)) worms were anesthetized with 0.25% tricaine  
524 and separated by sex. As controls, worms cultured in parallel were treated with an irrelevant dsRNA<sup>8</sup>. For RNA  
525 extraction, male worms were collected, excess media removed, and 100  $\mu\text{L}$  of TRIZOL was added. Parasites were  
526 then flash frozen in liquid N<sub>2</sub>, homogenized with a micro pestle, the volume of TRIZOL was brought to 600  $\mu\text{L}$  before  
527 RNA was purified using a Zymo Direct-zol RNA miniprep kit and processed for Illumina sequencing. RNAseq data  
528 was mapped to the *S. mansoni* genome (v7) using STAR and differential expression was analyzed by DESeq2 as  
529 previously described<sup>44</sup>. To define correlations between genes differentially regulated following RNAi of *tao* and/or  
530 *stk25*, we compiled a list of all genes that had significantly changed expression in either *stk*(RNAi) or *tao*(RNAi)  
531 datasets and plotted their log<sub>2</sub> fold-change expression in GraphPad Prism to calculate a Pearson's correlation  
532 coefficient. To evaluate the effects of *tao* and *stk25* RNAi on gene expression in specific tissues and cell types we  
533 collapsed related cell types from a *S. mansoni* single cell atlas<sup>29</sup> into 10 broad clusters of male somatic cell types  
534 (muscles, neurons, neoblasts, gut, etc.) (**Extended Data Fig. 9**). Genes highly enriched in these clusters were  
535 determined using Seurat v3.1.1<sup>45</sup> (parameters = logfc.threshold = 1, min.pct = 0.5) and compared to genes down-  
536 regulated ( $p \text{ adj} < 0.000001$ ) following both *tao* and *stk25* RNAi.

#### 537 538 **Purification of Recombinant STK25 and TAO**

539 Baculovirus expressing wildtype *Schistosoma mansoni* Smp\_068060 (TAO) or Smp\_096640 (STK25) with a C-  
540 terminal His<sub>6</sub> tag was generated by GenScript (Piscataway, NJ). cDNA encoding kinase-dead versions of both kinases  
541 were subcloned into the pFastBac1 vector with C-terminal His<sub>6</sub> tag and baculovirus was generated according to the  
542 manufacturer's instructions using the Bac-to-Bac Baculovirus Expression System (Invitrogen). Baculovirus was used  
543 as a 3<sup>rd</sup> pass virus to infect Sf9 cells grown in Gibco Sf 900 III SFM (ThermoFisher Scientific) supplemented with 1%  
544 FBS and Antibiotic-Antimycotic solution (Sigma-Aldrich). Cells were harvested 72hrs post infection for SmSTK25  
545 expression and 48hrs post infection for SmTAO expression. Frozen cell pellets were lysed with 20mM Tris, pH 8.0,  
546 5mM MgCl<sub>2</sub>, 300mM NaCl, 1% Triton X-100 (Fisher Scientific), DNase (24 $\mu\text{g}/\text{ml}$ ), 10% glycerol, 3mM 2-  
547 mercaptoethanol, and protease inhibitors (1 $\mu\text{g}/\text{ml}$  aprotinin, 2 $\mu\text{g}/\text{ml}$  leupeptin, 1mM benzamidine, and 0.2mM PMSF).  
548 After homogenization, the suspension was centrifuged for 1h at 186,000 x g and the supernatant was rotated with Ni<sup>2+</sup>-  
549 NTA resin (Qiagen) for 1.5hrs. The resin was washed, and the protein was eluted in 20mM Tris, pH 8.0, 5mM MgCl<sub>2</sub>,  
550 300mM NaCl, 0.05% Triton X-100, 10% glycerol, 3mM 2-mercaptoethanol, 150mM Imidazole, pH 8.0 and protease  
551 inhibitors (1 $\mu\text{g}/\text{ml}$  aprotinin, 2 $\mu\text{g}/\text{ml}$  leupeptin, 1mM benzamidine, and 0.2mM PMSF). Eluted proteins were either  
552 flash frozen or further dialyzed overnight into storage buffer (20mM Tris, pH 8.5, 5mM MgCl<sub>2</sub>, 150mM NaCl, 0.5mM  
553 DTT, 10% glycerol, and 1mM benzamidine) and flash frozen to -80°C.

554  
555 To generate an anti-SmSTK25 antibody, a C-terminal fragment of SmSTK25 corresponding to AA513-622 was  
556 amplified and sub-cloned into pET28 vector with a C-terminal His<sub>6</sub> tag for expression in *Escherichia coli*. This  
557 fragment was purified from transformed Rossetta 2 cells grown in LB medium and induced with 1mM isopropyl 1-  
558 thio-β-D-galactopyranoside for 16 hrs at 18°C. Cells were pelleted and resuspended into lysis buffer containing 50mM  
559 Tris, pH8.0, 300mM NaCl, 10% glycerol, and protease inhibitors (0.2mM PMSF, 2μg/ml aprotinin, and 2μg/ml  
560 leupeptin). The suspension was freeze-thawed and the following reagents were added to a final concentration of  
561 1mg/ml lysozyme, 1% Triton X-100, 5μg/ml DNase. After homogenization and sonication, lysate was centrifuged for  
562 40 min at 186,000 x g, and rotated with Ni<sup>2+</sup>-NTA resin for 1.5 hrs. The resin was washed, and protein was eluted in  
563 lysis buffer containing 300mM imidazole. SmSTK25 (513-622) was buffer-exchanged into 1X PBS and 10% glycerol  
564 and applied to a Superdex 200 column for gel filtration chromatography on an AKTA FPLC. The sample was  
565 processed at a flow rate of 0.9 ml/min in 1X PBS and 10% glycerol. Eluate was collected as 90 1-mL fractions on a  
566 Frac 900 fraction collector (Amersham Pharmacia) maintained at 4°C. Each fraction was assessed for protein and  
567 concentrated with an Amicon concentrator, 10-kDa cut-off (Millipore). Rabbit polyclonal antibodies were generated  
568 by Cocalico Biologicals, Inc.  
569

### 570 **Evaluation of kinase activity**

571 For kinase assays with radiolabeled ATP, STK25 or STK25K48R (1.7μM) were incubated alone or together with  
572 either TAO or TAOK57R (0.3μM) and 50μM ATP ([γ-<sup>32</sup>P]ATP, 6,000-9,000 cpm/pmol) in 10mM Tris, pH 8.0, and  
573 10mM MgCl<sub>2</sub> for 10 min at 30°C. Following gel electrophoresis and autoradiography, STK25 or  
574 STK25K48R(1.25μM) as well as TAO or TAOK57R (0.25μM) bands were excised and analyzed by scintillation  
575 counting (Perkin Elmer, Tri-Carb 2910TR). For evaluation of STK25 phosphorylation by western blotting, proteins  
576 were incubated for 30 mins at 30°C in kinase assay buffer (10 mM Tris pH 8.0, 10 mM MgCl<sub>2</sub>, 0.5 μM per protein)  
577 with or without 50 μM ATP in a reaction volume of 30 μL. Reactions were quenched with 10μL of 4x Laemmli buffer  
578 and samples boiled at 99°C for 4 min, then stored at -20°C. Proteins were resolved by SDS-PAGE (Bio-Rad 4-20%  
579 precast polyacrylamide gel, cat# 4568095) for 45 min at 140V. The gel was placed in cold transfer buffer (25 mM  
580 Tris, 192 mM Glycine, 10% (v/v) methanol, pH ~8.4) and transferred to a nitrocellulose membrane (Bio-Rad cat#  
581 1620115) for 60 min at 100V, 4°C. The membrane was stained with Ponceau S Solution (Sigma cat# P7170) for 5  
582 min, imaged and destained by 2x washes with TBST (20 mM Tris, 150 mM NaCl, 0.1% (v/v) Tween20). The  
583 membrane was blocked for 1hr at RT with blocking buffer (Odyssey Blocking Buffer, Li-Cor cat# 927-40000) diluted  
584 1:5 in TBS (20 mM Tris, 150 mM NaCl), then stained O/N at 4°C with primary antibody diluted in blocking buffer.  
585 Membrane was washed 3x 5 min with TBST, then stained with secondary antibody diluted in blocking buffer, 1hr at  
586 RT. Membrane was washed 3x 5 min with TBST, then imaged with a LI-COR Odyssey imaging system. Primary  
587 antibodies were as follows: to detect phosphorylated T173 of smSTK25 and kinase-dead smSTK25, we used Rabbit-  
588 anti-MST4 + MST3 + STK25 (phospho T174 + T178 + T190) antibody [EP2123Y] (ab76579) from Abcam. To detect  
589 total smSTK25 and kinase-dead smSTK25 we used the Rabbit polyclonal antibody against the STK25 C-terminus  
590 described above. Secondary antibody for all blots was LI-COR IRDYE 680 red, Goat anti-Rabbit cat# 925-68071,  
591 and was used at a dilution of 1:10,000.

592 For mass spectrometry analyses of SmTAO phosphorylation of kinase-dead SmSTK25, kinase reactions were  
593 performed as above, and the SmSTK protein was excised from an SDS-PAGE gel and the protein was analyzed by  
594 the UT Southwestern Proteomics Core. Specifically, protein gel pieces were digested overnight with trypsin (Pierce)  
595 following reduction and alkylation with DTT and iodoacetamide (Sigma–Aldrich). The samples then underwent solid-  
596 phase extraction cleanup with Oasis HLB plates (Waters) and the resulting samples were analyzed by LC/MS/MS,  
597 using an Orbitrap Fusion Lumos mass spectrometer (Thermo Electron) coupled to an Ultimate 3000 RSLC-Nano  
598 liquid chromatography systems (Dionex). Samples were injected onto a 75 μm i.d., 75-cm long EasySpray column  
599 (Thermo), and eluted with a gradient from 1-28% buffer B over 90 min. Buffer A contained 2% (v/v) ACN and 0.1%  
600 formic acid in water, and buffer B contained 80% (v/v) ACN, 10% (v/v) trifluoroethanol, and 0.1% formic acid in  
601 water. The mass spectrometer operated in positive ion mode with a source voltage of 1.8 kV and an ion transfer tube  
602 temperature of 275 °C. MS scans were acquired at 120,000 resolution in the Orbitrap and up to 10 MS/MS spectra  
603 were obtained in the ion trap for each full spectrum acquired using higher-energy collisional dissociation (HCD) for  
604 ions with charges 2-7. Dynamic exclusion was set for 25 s after an ion was selected for fragmentation. Raw MS data  
605 files were converted to a peak list format and analyzed using the central proteomics facilities pipeline (CPFP), version  
606 2.0.3<sup>46,47</sup>. Peptide identification was performed using the X!Tandem<sup>48</sup> and open MS search algorithm (OMSSA)<sup>49</sup>  
607 search engines against the human protein database from Uniprot, with common contaminants and reversed decoy  
608 sequences appended<sup>50</sup>. Fragment and precursor tolerances of 10 ppm and 0.6 Da were specified, and three missed

609 cleavages were allowed. Carbamidomethylation of Cys was set as a fixed modification with oxidation of Met and  
610 phosphorylation of Ser, Thr, and Tyr set as variable modifications. Phosphorylation sites were localized using the  
611 ModLS algorithm, using cutoff values for positive site identification that represent a scenario where the false discovery  
612 rate is  $< 1\%$  <sup>51</sup>.

613

#### 614 **Gene Ontology (GO)**

615 The Gene Ontology (GO) annotation for *Schistosoma mansoni* was obtained from GeneDB  
616 (<https://www.genedb.org/>). GO term enrichment was performed using the weight01 method provided in topGO  
617 (v2.34.0) for biological process (BP), molecular function (MF) and cellular component (CC). For each category, the  
618 analysis was restricted to terms with a node size of  $\geq 5$ . Fisher's exact test was applied to assess the significance of  
619 overrepresented terms compared with the screened genes. The threshold was set as  $FDR < 0.05$ .

620

#### 621 **Identification of *S. mansoni*-specific phenotypes**

622 For data in **Supplementary Table 5**, orthologs of *S. mansoni* genes in *C. elegans*, *D. melanogaster* and human were  
623 identified from WormBase ParaSite<sup>52</sup>. We considered *S. mansoni* and *Schmidtea mediterranea* genes (taking the  
624 dd\_Smed\_v6 gene set from PlanMine<sup>53</sup>) to be one-to-one orthologs if they were each other's top BLASTP hits, with  
625  $E$ -value  $< 0.05$ , and the BLAST  $E$ -value of the top BLASTP hit was  $10^5$  times lower than the BLAST  $E$ -value for the  
626 next best hit. *C. elegans* RNAi/mutant phenotypes were identified from WormBase<sup>54</sup> and *D. melanogaster* phenotypes  
627 from FlyBase<sup>55</sup>.

628

629

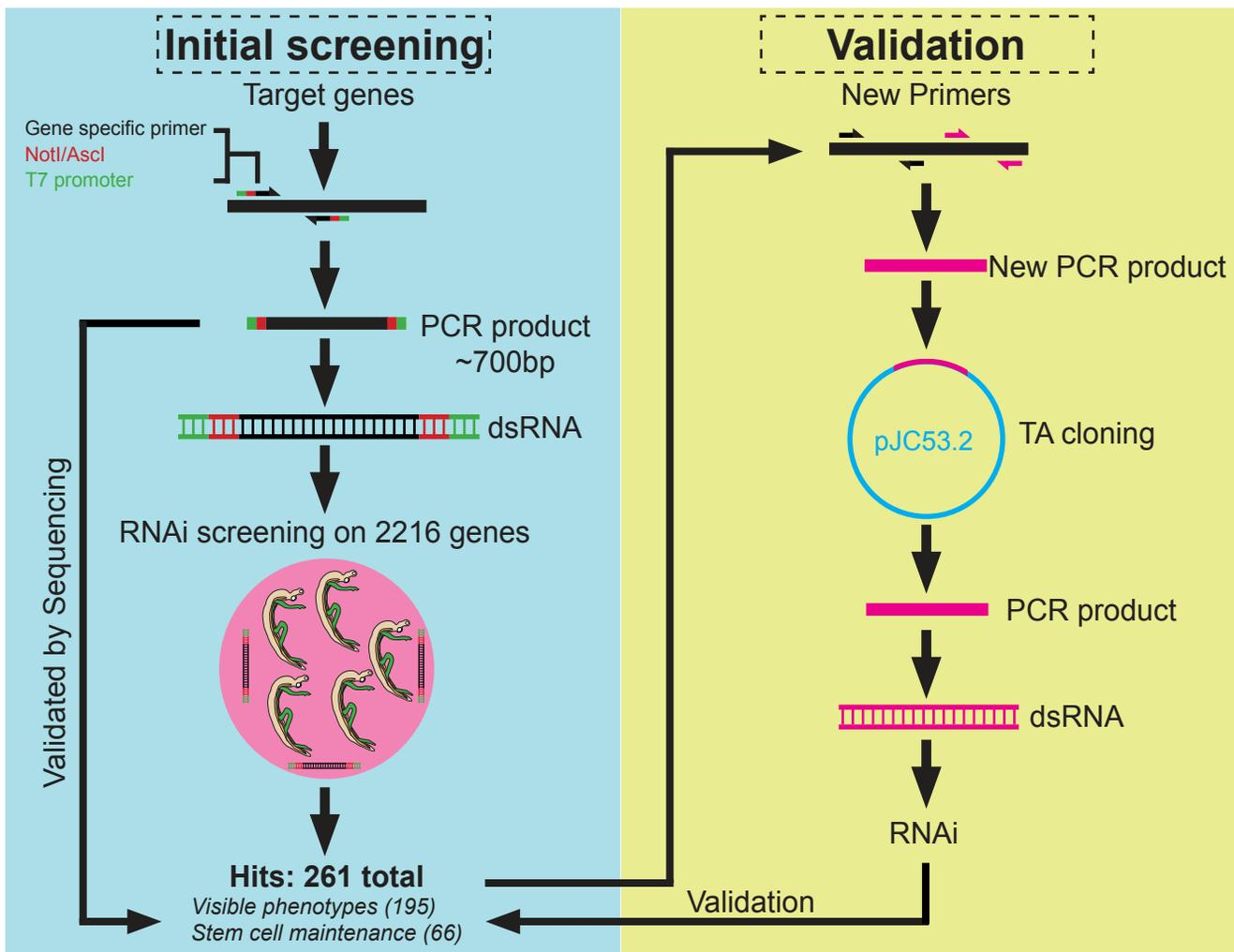
630

631

- 632 1 Berriman, M. *et al.* The genome of the blood fluke *Schistosoma mansoni*. *Nature* **460**, 352-358,  
633 doi:10.1038/nature08160 (2009).
- 634 2 Young, N. D. *et al.* Whole-genome sequence of *Schistosoma haematobium*. *Nat Genet* **44**, 221-225,  
635 doi:10.1038/ng.1065 (2012).
- 636 3 The *Schistosoma japonicum* Genome Sequencing and Functional Analysis Consortium. The *Schistosoma*  
637 *japonicum* genome reveals features of host-parasite interplay. *Nature* **460**, 345-351, doi:10.1038/nature08140  
638 (2009).
- 639 4 Guidi, A. *et al.* Application of RNAi to Genomic Drug Target Validation in Schistosomes. *PLoS Negl Trop*  
640 *Dis* **9**, e0003801, doi:10.1371/journal.pntd.0003801 (2015).
- 641 5 Mourao, M. M., Dinguirard, N., Franco, G. R. & Yoshino, T. P. Phenotypic screen of early-developing larvae  
642 of the blood fluke, *Schistosoma mansoni*, using RNA interference. *PLoS Negl Trop Dis* **3**, e502,  
643 doi:10.1371/journal.pntd.0000502 (2009).
- 644 6 Collins, J. J., Wendt, G. R., Iyer, H. & Newmark, P. A. Stem cell progeny contribute to the schistosome host-  
645 parasite interface. *Elife* **5**, doi:10.7554/eLife.12473 (2016).
- 646 7 Collins, J. N. & Collins, J. J., 3rd. Tissue Degeneration following Loss of *Schistosoma mansoni cbp1* Is  
647 Associated with Increased Stem Cell Proliferation and Parasite Death In Vivo. *PLoS Pathog* **12**, e1005963,  
648 doi:10.1371/journal.ppat.1005963 (2016).
- 649 8 Collins, J. J., III *et al.* Adult somatic stem cells in the human parasite *Schistosoma mansoni*. *Nature* **494**, 476-  
650 479, doi:10.1038/nature11924 (2013).
- 651 9 Pearce, E. J. & MacDonald, A. S. The immunobiology of schistosomiasis. *Nat Rev Immunol* **2**, 499-511,  
652 doi:10.1038/nri843 (2002).
- 653 10 Wang, J., Chen, R. & Collins, J. J., 3rd. Systematically improved in vitro culture conditions reveal new  
654 insights into the reproductive biology of the human parasite *Schistosoma mansoni*. *PLoS Biol* **17**, e3000254,  
655 doi:10.1371/journal.pbio.3000254 (2019).
- 656 11 Buszczak, M., Signer, R. A. & Morrison, S. J. Cellular differences in protein synthesis regulate tissue  
657 homeostasis. *Cell* **159**, 242-251, doi:10.1016/j.cell.2014.09.016 (2014).
- 658 12 Kamath, R. S. *et al.* Systematic functional analysis of the *Caenorhabditis elegans* genome using RNAi.  
659 *Nature* **421**, 231-237, doi:10.1038/nature01278 (2003).
- 660 13 Reddien, P. W., Bermange, A. L., Murfitt, K. J., Jennings, J. R. & Sanchez Alvarado, A. Identification of  
661 genes needed for regeneration, stem cell function, and tissue homeostasis by systematic gene perturbation in  
662 planaria. *Dev Cell* **8**, 635-649, doi:10.1016/j.devcel.2005.02.014 (2005).
- 663 14 Bibo-Verdugo, B. *et al.* The Proteasome as a Drug Target in the Metazoan Pathogen, *Schistosoma mansoni*.  
664 *ACS Infect Dis*, doi:10.1021/acsinfecdis.9b00237 (2019).
- 665 15 Nabhan, J. F., El-Shehabi, F., Patocka, N. & Ribeiro, P. The 26S proteasome in *Schistosoma mansoni*:  
666 bioinformatics analysis, developmental expression, and RNA interference (RNAi) studies. *Exp Parasitol*  
667 **117**, 337-347, doi:10.1016/j.exppara.2007.08.002 (2007).
- 668 16 Meyer, H. & Wehl, C. C. The VCP/p97 system at a glance: connecting cellular function to disease  
669 pathogenesis. *J Cell Sci* **127**, 3877-3883, doi:10.1242/jcs.093831 (2014).
- 670 17 Bard, J. A. M. *et al.* Structure and Function of the 26S Proteasome. *Annu Rev Biochem* **87**, 697-724,  
671 doi:10.1146/annurev-biochem-062917-011931 (2018).
- 672 18 Mendez, D. *et al.* ChEMBL: towards direct deposition of bioassay data. *Nucleic Acids Res* **47**, D930-D940,  
673 doi:10.1093/nar/gky1075 (2019).
- 674 19 Marcellino, C. *et al.* WormAssay: a novel computer application for whole-plate motion-based screening of  
675 macroscopic parasites. *PLoS Negl Trop Dis* **6**, e1494, doi:10.1371/journal.pntd.0001494 (2012).
- 676 20 Rojo-Arreola, L. *et al.* Chemical and genetic validation of the statin drug target to treat the helminth disease,  
677 schistosomiasis. *PLoS One* **9**, e87594, doi:10.1371/journal.pone.0087594 (2014).
- 678 21 Anderson, D. J. *et al.* Targeting the AAA ATPase p97 as an Approach to Treat Cancer through Disruption  
679 of Protein Homeostasis. *Cancer Cell* **28**, 653-665, doi:10.1016/j.ccell.2015.10.002 (2015).
- 680 22 Magnaghi, P. *et al.* Covalent and allosteric inhibitors of the ATPase VCP/p97 induce cancer cell death. *Nat*  
681 *Chem Biol* **9**, 548-556, doi:10.1038/nchembio.1313 (2013).
- 682 23 Newton, K. *et al.* Ubiquitin chain editing revealed by polyubiquitin linkage-specific antibodies. *Cell* **134**,  
683 668-678, doi:10.1016/j.cell.2008.07.039 (2008).
- 684 24 Khare, S. *et al.* Proteasome inhibition for treatment of leishmaniasis, Chagas disease and sleeping sickness.  
685 *Nature* **537**, 229-233, doi:10.1038/nature19339 (2016).
- 686 25 Li, H. *et al.* Structure- and function-based design of *Plasmodium*-selective proteasome inhibitors. *Nature*  
687 **530**, 233-236, doi:10.1038/nature16936 (2016).

- 688 26 Ceccarelli, D. F. *et al.* CCM3/PDCD10 heterodimerizes with germinal center kinase III (GCKIII) proteins  
689 using a mechanism analogous to CCM3 homodimerization. *J Biol Chem* **286**, 25056-25064,  
690 doi:10.1074/jbc.M110.213777 (2011).
- 691 27 Poon, C. L. C. *et al.* A Hippo-like Signaling Pathway Controls Tracheal Morphogenesis in *Drosophila*  
692 *melanogaster*. *Dev Cell* **47**, 564-575 e565, doi:10.1016/j.devcel.2018.09.024 (2018).
- 693 28 Preisinger, C. *et al.* YSK1 is activated by the Golgi matrix protein GM130 and plays a role in cell migration  
694 through its substrate 14-3-3zeta. *J Cell Biol* **164**, 1009-1020, doi:10.1083/jcb.200310061 (2004).
- 695 29 Wendt, G. R. *et al.* A single-cell RNAseq atlas of the pathogenic stage of *Schistosoma mansoni* identifies a  
696 key regulator of blood feeding. *bioRxiv*, doi:doi.org/10.1101/2020.02.03.932004 (2020).
- 697 30 Amrutkar, M. *et al.* Genetic Disruption of Protein Kinase STK25 Ameliorates Metabolic Defects in a Diet-  
698 Induced Type 2 Diabetes Model. *Diabetes* **64**, 2791-2804, doi:10.2337/db15-0060 (2015).
- 699 31 Alsford, S. *et al.* High-throughput phenotyping using parallel sequencing of RNA interference targets in the  
700 African trypanosome. *Genome Res* **21**, 915-924, doi:10.1101/gr.115089.110 (2011).
- 701 32 Bushell, E. *et al.* Functional Profiling of a *Plasmodium* Genome Reveals an Abundance of Essential Genes.  
702 *Cell* **170**, 260-272 e268, doi:10.1016/j.cell.2017.06.030 (2017).
- 703 33 Sidik, S. M. *et al.* A Genome-wide CRISPR Screen in *Toxoplasma* Identifies Essential Apicomplexan Genes.  
704 *Cell* **166**, 1423-1435 e1412, doi:10.1016/j.cell.2016.08.019 (2016).
- 705 34 Janes, J. *et al.* The ReFRAME library as a comprehensive drug repurposing library and its application to the  
706 treatment of cryptosporidiosis. *Proc Natl Acad Sci U S A* **115**, 10750-10755, doi:10.1073/pnas.1810137115  
707 (2018).
- 708 35 Basch, P. F. Cultivation of *Schistosoma mansoni* *in vitro*. I. Establishment of cultures from cercariae and  
709 development until pairing. *J Parasitol* **67**, 179-185 (1981).
- 710 36 Collins, J. J., III *et al.* Genome-Wide Analyses Reveal a Role for Peptide Hormones in Planarian Germline  
711 Development. *PLoS Biol* **8**, e1000509 (2010).
- 712 37 Collins, J. J., III, King, R. S., Cogswell, A., Williams, D. L. & Newmark, P. A. An atlas for *Schistosoma*  
713 *mansoni* organs and life-cycle stages using cell type-specific markers and confocal microscopy. *PLoS Negl*  
714 *Trop Dis* **5**, e1009, doi:10.1371/journal.pntd.0001009 (2011).
- 715 38 International Helminth Genomes Consortium. Comparative genomics of the major parasitic worms. *Nat*  
716 *Genet* **51**, 163-174, doi:10.1038/s41588-018-0262-1 (2019).
- 717 39 Lamore, S. D. *et al.* Deconvoluting Kinase Inhibitor Induced Cardiotoxicity. *Toxicol Sci* **158**, 213-226,  
718 doi:10.1093/toxsci/kfx082 (2017).
- 719 40 Lynch, J. J., 3rd, Van Vleet, T. R., Mittelstadt, S. W. & Blomme, E. A. G. Potential functional and  
720 pathological side effects related to off-target pharmacological activity. *J Pharmacol Toxicol Methods* **87**,  
721 108-126, doi:10.1016/j.vascn.2017.02.020 (2017).
- 722 41 Bowes, J. *et al.* Reducing safety-related drug attrition: the use of *in vitro* pharmacological profiling. *Nat Rev*  
723 *Drug Discov* **11**, 909-922, doi:10.1038/nrd3845 (2012).
- 724 42 Whatley, K. C. L. *et al.* The repositioning of epigenetic probes/inhibitors identifies new anti-schistosomal  
725 lead compounds and chemotherapeutic targets. *PLoS Negl Trop Dis* **13**, e0007693,  
726 doi:10.1371/journal.pntd.0007693 (2019).
- 727 43 Whiteland, H. L. *et al.* An *Abies procera*-derived tetracyclic triterpene containing a steroid-like nucleus core  
728 and a lactone side chain attenuates *in vitro* survival of both *Fasciola hepatica* and *Schistosoma mansoni*. *Int*  
729 *J Parasitol Drugs Drug Resist* **8**, 465-474, doi:10.1016/j.ijpddr.2018.10.009 (2018).
- 730 44 Wendt, G. R. *et al.* Flatworm-specific transcriptional regulators promote the specification of tegumental  
731 progenitors in *Schistosoma mansoni*. *Elife* **7**, doi:10.7554/eLife.33221 (2018).
- 732 45 Stuart, T. *et al.* Comprehensive Integration of Single-Cell Data. *Cell* **177**, 1888-1902 e1821,  
733 doi:10.1016/j.cell.2019.05.031 (2019).
- 734 46 Trudgian, D. C. & Mirzaei, H. Cloud CFP: a shotgun proteomics data analysis pipeline using cloud and  
735 high performance computing. *J Proteome Res* **11**, 6282-6290, doi:10.1021/pr300694b (2012).
- 736 47 Trudgian, D. C. *et al.* CFP: a central proteomics facilities pipeline. *Bioinformatics* **26**, 1131-1132,  
737 doi:btq081 [pii]  
738 10.1093/bioinformatics/btq081 (2010).
- 739 48 Craig, R. & Beavis, R. C. TANDEM: matching proteins with tandem mass spectra. *Bioinformatics* **20**, 1466-  
740 1467, doi:10.1093/bioinformatics/bth092 (2004).
- 741 49 Geer, L. Y. *et al.* Open mass spectrometry search algorithm. *Journal of proteome research* **3**, 958-964,  
742 doi:10.1021/pr0499491 (2004).

743 50 Elias, J. E. & Gygi, S. P. Target-decoy search strategy for increased confidence in large-scale protein  
744 identifications by mass spectrometry. *Nature methods* **4**, 207-214, doi:10.1038/nmeth1019 (2007).  
745 51 Trudgian, D. C., Singleton, R., Cockman, M. E., Ratcliffe, P. J. & Kessler, B. M. ModLS: post-translational  
746 modification localization scoring with automatic specificity expansion. *J. Proteomics Bioinform* **5**, 283-289  
747 (2012).  
748 52 Bolt, B. J. *et al.* Using WormBase ParaSite: An Integrated Platform for Exploring Helminth Genomic Data.  
749 *Methods Mol Biol* **1757**, 471-491, doi:10.1007/978-1-4939-7737-6\_15 (2018).  
750 53 Rozanski, A. *et al.* PlanMine 3.0-improvements to a mineable resource of flatworm biology and biodiversity.  
751 *Nucleic Acids Res* **47**, D812-D820, doi:10.1093/nar/gky1070 (2019).  
752 54 Harris, T. W. *et al.* WormBase: a modern Model Organism Information Resource. *Nucleic Acids Res* **48**,  
753 D762-D767, doi:10.1093/nar/gkz920 (2020).  
754 55 Thurmond, J. *et al.* FlyBase 2.0: the next generation. *Nucleic Acids Res* **47**, D759-D765,  
755 doi:10.1093/nar/gky1003 (2019).  
756

**Fig. 1****a****b**

Adult Schistosomes

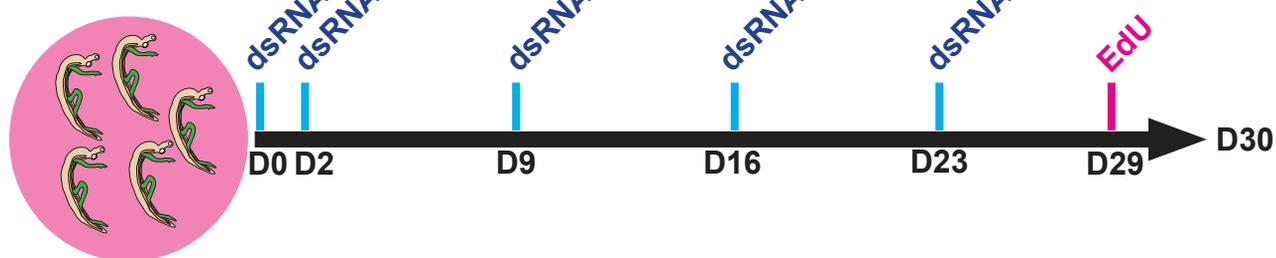
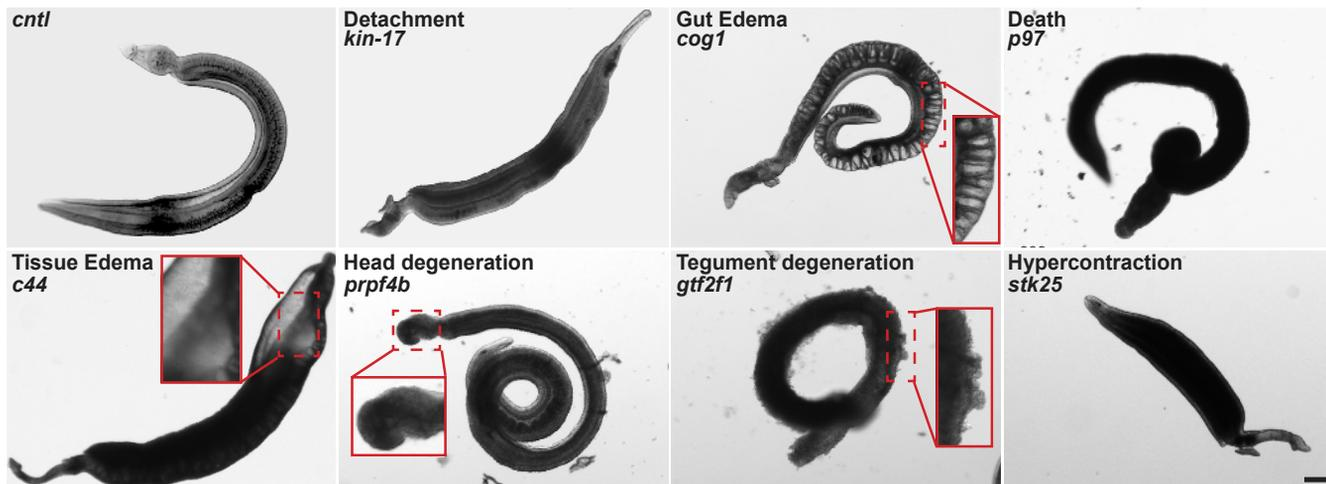
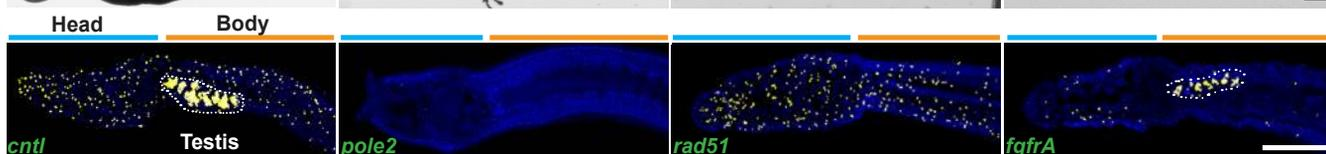


# Fig. 2

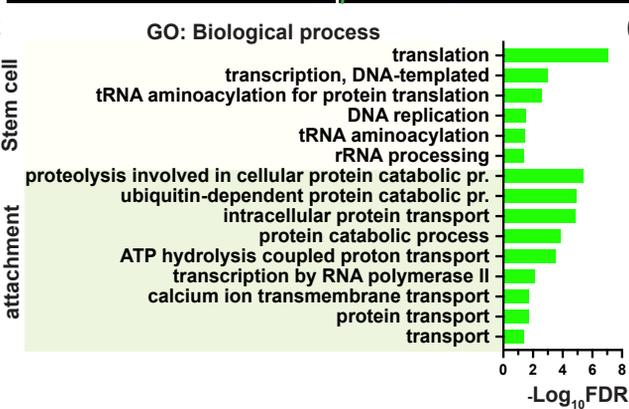
**a**



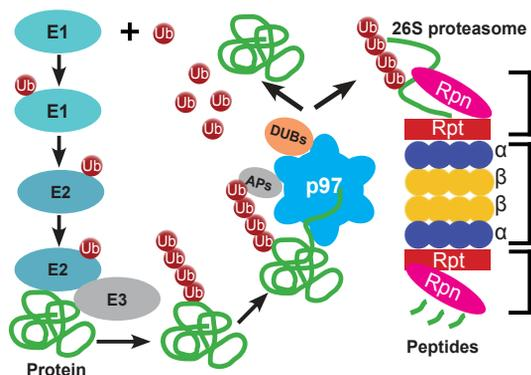
**b**

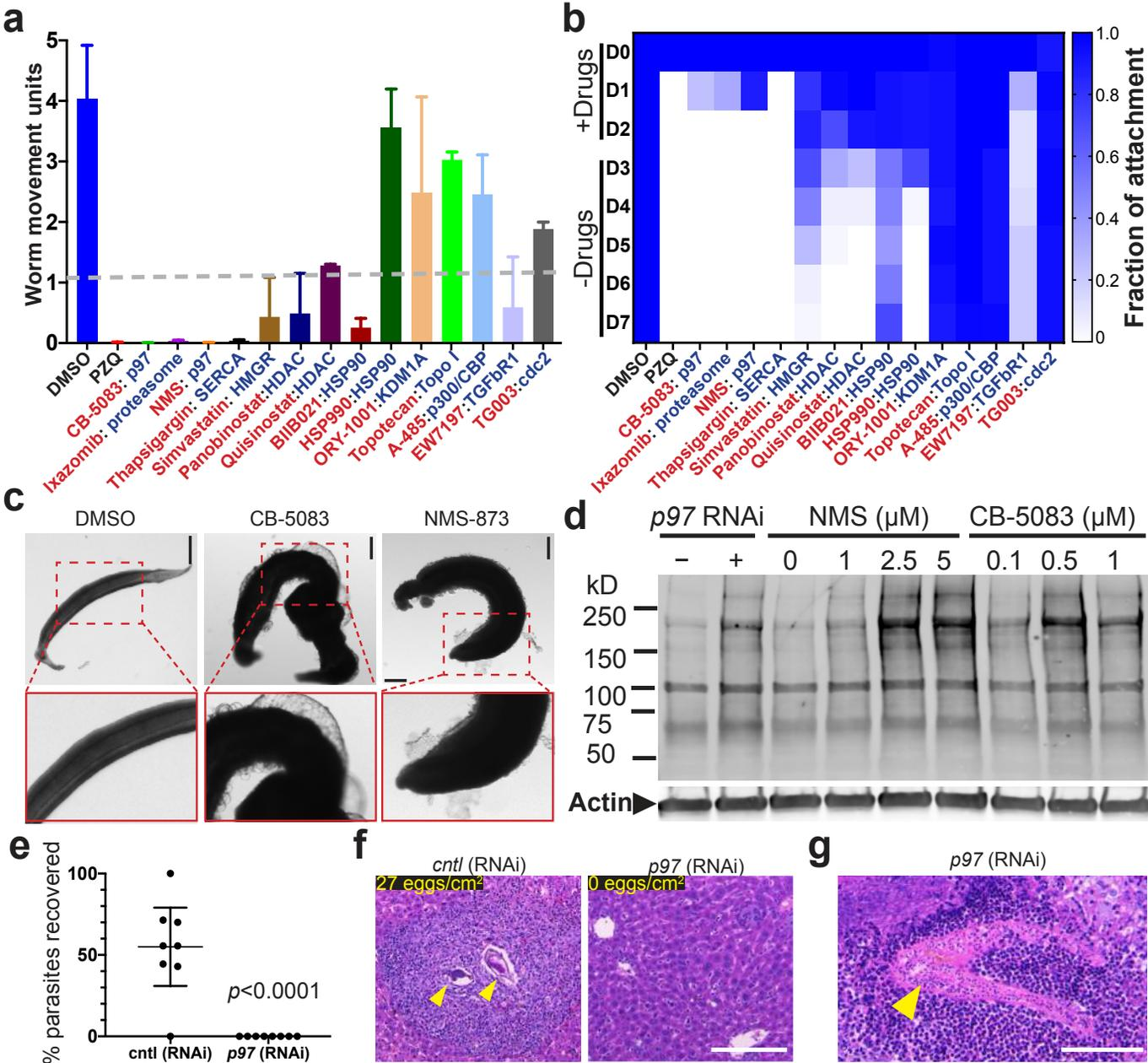


**c**



**d**



**Fig. 3**

**Fig. 4**